IL NUOVO CIMENTO **45 C** (2022) 55
DOI 10.1393/ncc/i2022-22055-2

COLLOQUIA: IWM-EC 2021

Status of data analysis and preliminary results of the CHIFAR experiment

P. RUSSOTTO(1)(*), E. DE FILIPPO(2), E. V. PAGANO(1), E. GERACI(2)(3), C. MAIOLINO(1), N. S. MARTORANA(1)(3), L. ACOSTA(2)(4), T. CAP(5), G. CARDELLA(2), F. FAVELA(1)(6), B. GNOFFO(2)(3), C. GUAZZONI(7), G. LANZALONE(1)(8), T. MATULEWICZ(9), A. PAGANO(2), M. PAPA(2), K. PIASECKI(9), S. PIRRONE(2), R. PLANETA(10), G. POLITI(2)(3), F. RISITANO(2)(11), F. RIZZO(1)(3), V. SICARI(7), K. SIWEK-WILCZYNSKA(9), I. SKWIRA-CHALOT(9) and M. TRIMARCHI(2)(11)

(1) *INFN, Laboratori Nazionali del Sud - Catania, Italy*
(2) *INFN, Sezione di Catania - Catania, Italy*
(3) *Dipartimento di Fisica e Astronomia "E. Majorana", Università di Catania - Catania, Italy*
(4) *Instituto de Fisica, Universidad Nacional Autònoma de México - Mexico City, Mexico*
(5) *National Centre for Nuclear Research - Otwock-Swierk, Poland*
(6) *Instituto de Ciencias Nucleares, Universidad Nacional Autònoma de México - Mexico City, Mexico*
(7) *Dip. di Elettronica, Informazione e Bioingegneria, Politecnico di Milano - Milano, Italy*
(8) *Facoltà di Ingegneria e Architettura, Università Kore - Enna, Italy*
(9) *Faculty of Physics, University of Warsaw - Warsaw, Poland*
(10) *M. Smoluchowski Institute of Physics, Jagiellonian University - Krakow, Poland*
(11) *Dipartimento di Scienze MIFT, Univ. di Messina - Messina, Italy*

received 12 May 2022

Summary. — In the CHIFAR experiment, carried out at the INFN-LNS laboratory, we studied reactions between beams of ^{124}Sn, ^{124}Xe and ^{112}Sn, accelerated at 20 AMeV, and targets of ^{64}Ni, ^{64}Zn and ^{58}Ni by using the CHIMERA multi-detector coupled to 10 telescopes of the FARCOS array. The main topics of the experiment are the competition between reaction mechanisms and the Intermediate Mass Fragment production phenomenon, aiming to extend towards the low energy regime the studies performed in previous CHIMERA experiments carried out at beam energy of 35 AMeV. Status of data analysis and preliminary results will be presented.

(*) E-mail: russotto@lns.infn.it

1. – Introduction

Data analysis of past experiments carried out at INFN-LNS by using the 4π CHIMERA multi-detector [1] allowed to give a clear picture of competition among reaction mechanisms and of Intermediate Mass Fragments (IMF) emission in Heavy-Ion reaction at the beam energy of 35 AMeV. In semi-peripheral reactions, evidence of production of lighter IMFs with $3 \leq Z \lesssim 10$ from neck-fragmentation mechanisms, taking place in short times after the beginning of re-separation between the projectile-like and target-like fragments (PLF and TLF), were given by observing the deviation of relative velocities from the ones due to Coulomb repulsion and a high degree of alignment of reaction products [2-4]. Moreover, the neutron enrichment of IMFs, driven by the isospin migration process, also allowed inferring properties of the symmetry energy of the nuclear Equation Of State at low densities [5]. Emission of heavier IMFs was found to take place in longer times in a, however, fast and non-equilibrated break-up of the PLF, the "dynamical fission" [3,6-8]. In this case, the evidence of dynamical effects was the prevalence of an alignment, to the PLF direction before the break-up, of the PLF break-up products and the velocity deviation from the Coulomb one. These mechanisms competed with the equilibrated emission of IMFs taking place on even longer timescales. A detailed study also showed that the strength of dynamical effects increases with the isospin content of, both, projectile and target, giving evidence of an important dependence of the reaction mechanism evolution on the initial neutron richness of the colliding nuclei [9]. Moreover, in the central collisions, evidence of a multi-fragmentation pattern was found, with the gas phase neutron richer than the liquid one [10].

The CHIFAR experiment was carried out at LNS in order to extend these studies toward the lower energy regime and shed light on how the above mentioned effects evolve when lowering the initial relative energy of the system. Reactions between beams of ^{124}Sn, ^{124}Xe and ^{112}Sn, accelerated at 20 AMeV by the Super-Conductive Cyclotron, and targets of ^{64}Ni, ^{64}Zn and ^{58}Ni were studied by using the CHIMERA multi-detector [11,12] coupled to 10 telescopes of the FARCOS array [13, 14]. The 10 FARCOS telescopes, grouped in 5 couples, were arranged in a ring-like configuration covering about 3/4 of the 2π azimuthal range at polar angles, in the laboratory, between 16 and 30 degrees. Just as an example, interesting studies at similar energy and in the same range of masses of nuclei here studied were already performed in the past and published in [15,16]. In our case, the different combinations of neutron-rich and neutron-poor projectiles and targets will allow, also, to investigate the above-mentioned topics with respect to the entrance channel Isospin content.

Here we report on the status of data reduction and present some preliminary results.

2. – Status of data analysis and preliminary results

For most of the CHIFAR experiment, data were collected by requiring at least 2 CHIMERA Silicon detectors fired. When needed, data were also collected by using a dedicated trigger for the FARCOS telescopes. We will report here only on the status of the analysis of data collected by using CHIMERA multi-detector. Data shown here are not filtered for detector response, thus when interpreting results attention has to be paid to possible biases arising from geometrical and intrinsic efficiencies. Preliminary results of data collected by FARCOS are reported in [17]. The identifications of particles by means of ΔE-E and E-ToF (for particles stopped in the Silicon detectors) techniques are nearly to be completed and have been used for the results presented here. Vice versa, info

obtainable by the identification of Light Charged Particles using Pulse Shape Analysis (PSA) on CsI(Tl) signal and by the identification of particles stopped in the Silicon detectors by means of the PSA on Silicon signal have not been included here. Differing from most of the previous CHIMERA experiments, the lower energy and heavy projectiles and targets of the CHIFAR experiment result in most of the particles, including the heavier ones, being stopped in the Silicon detectors, demanding to the E-ToF techniques the major role as identification technique. For this reason, careful attention has been dedicated to this phase of the identification procedures, upgrading the methods previously used; more details are available in ref. [18]. As a preliminary result, the mass number, A, *vs.* component of the velocity parallel to the beam axis, v_{par}, as obtained for the ^{124}Sn + ^{64}Ni reaction at 20 AMeV for events where two fragments having $A \geq 6$ were detected, is shown in the left panel of fig. 1. The events with multiplicity greater than two, given the current status of calibration procedures, are less than ∼10% of the ones with multiplicity equal to two and are not included here. In the figure, we can see the region of quasi-elastically scattered projectiles having parallel velocities similar to the beam one and mass near the one of the projectile. Here some imperfections related to the use of the E-ToF technique can be noticed: the shape observed in the high-populated PLF region indicates the presence of an auto-correlation in the data, *i.e.*, biggest masses have lowest velocities and vice versa. However, the good reproduction of the masses in the region of $A \sim 120$ can be taken as a satisfactory result. Opposite to the PLF, the TLF can also be seen at very low velocities and with a wide mass distribution around A∼64. This is a good result too, given the short base-of-flight (40 cm) of CHIMERA detectors in that angular region. In addition to the PLF-TLF quasi-elastic scattering, expected to be the main pattern in the peripheral collisions, we also see a strong populated region of heavy fragments with a velocity slightly below the beam one. To better understand the observed pattern, the right panel of fig. 1, shows, event-by-event, the sum of the mass of the couple of fragments, $A_1 + A_2$, of the left panel *vs.* the component of velocity parallel to the beam axis of their c.m. system, $\vec{v} = \frac{A_1 \cdot \vec{v_1} + A_2 \cdot \vec{v_2}}{A_1 + A_2}$. There we can recognize the region of completely detected events, with a mass number around ∼188 and parallel velocity near to the projectile-target c.m. ref. sys., and a high populated second region

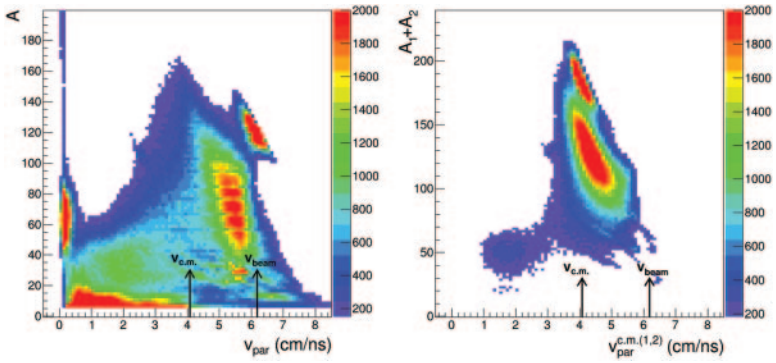

Fig. 1. – (Color online) Left: mass number (A) as a function of the component of velocity parallel to the beam axis (v_{par}) for the events where two fragments of $A \geq 6$ were detected by the CHIMERA detector in the ^{124}Sn + ^{64}Ni collisions at 20 AMeV beam energy. The black arrows indicate the beam and c.m. velocities. Right: sum of mass numbers for the two fragments of the left panel *vs.* their centre of mass component of velocity parallel to the beam axis.

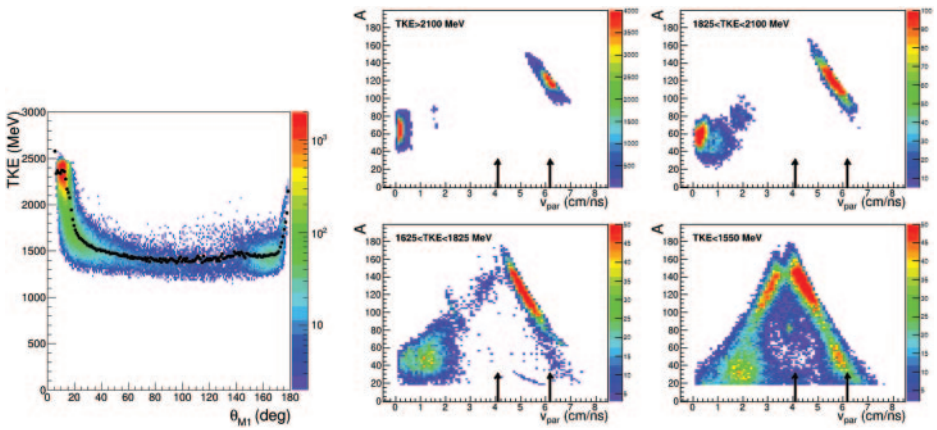

Fig. 2. – (Color online) Left: Total Kinetic Energy (TKE) as a function of polar deflection angle θ_{M1} of the heavier fragment, in the c.m. reference system, for the subset of complete events. Right (4 panels): mass number *vs.* the component of velocity parallel to the beam axis for the two fragments, for different selections of TKE interval, from peripheral events (highest TKE) to central events (lowest TKE).

of incomplete events with velocity intermediate between the projectile and c.m. ones and mass around ∼124, containing also the events where only the PLF products were detected. For the case of completely detected events, the relation between Total Kinetic Energy, TKE, and polar deflection angle of the heavier of the two fragments in the c.m. ref. sys, θ_{M1}, is shown in the left panel of fig. 2; the expected pattern, evolving from quasi elastic collisions, with high TKE and low deflection angles, to Deep-Inelastic Collisions (DIC) with a higher degree of dissipation and higher deflection angles, up to fully damped collisions with low TKE and "almost flat" deflection angle distribution, is seen. In the right panel of fig. 2 we present, for the same class of events of the left panel, the A *vs.* v_{par} for the two fragments, for different selections of the TKE. We can see the evolution from quasi-elastic scattering for higher TKE, to a DIC behaviour for intermediate TKE, to a fusion-fission pattern for low TKE-central events. Here the lower population of the "slower arm", with respect to the "faster" one, is ascribed to the lack of data in CHIMERA due to the shadow of the FARCOS telescopes on CHIMERA detectors. It follows that the strong populated region of heavy fragments with a velocity slightly below the beam one in the left panel of fig. 1 includes the PLFs after DIC, fast products of fusion-fission reactions and, also, the heavier remnant of the PLF break-up in the events where the TLF was not detected. Thus, the PLF break-up events, following a DIC, have to be searched among the events populating the region of incomplete events in the right panel of fig. 1.

A full description of the procedure used to select the PLF break-up events will be given in future publications and is briefly reported here. We selected those events where two fragments with $v_{par} > 2.15\,\mathrm{cm/ns}$ were detected, to reject TLF and, partially, fragments emitted by the TLF, and where the relative velocity between the two fragments was compatible, up to a 30% deviation, with the one expected in an equilibrated break-up as given by the Viola systematics [19]. Please note that here events with total multiplicity greater than two can be included in the selection. In addition, since we want the two fragments to be the results of the PLF break-up, we requested the sum of their masses

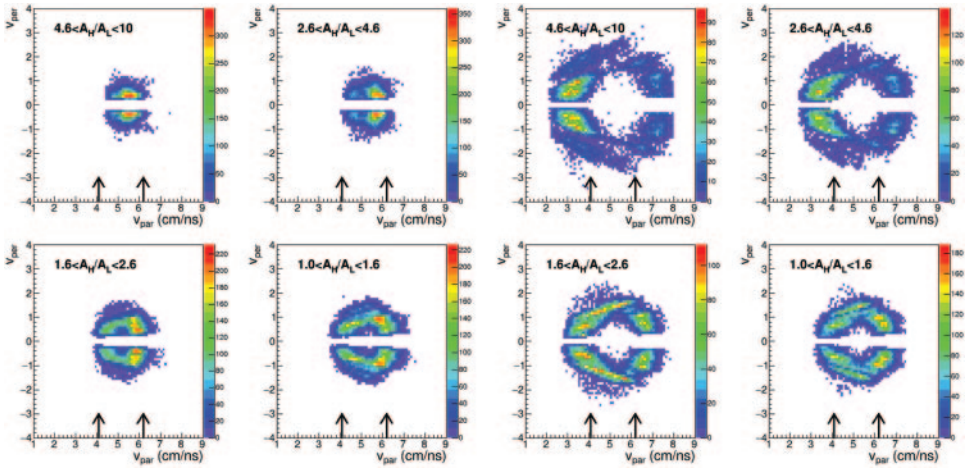

Fig. 3. – (Color online) Left (4 panels): component of velocity perpendicular (v_{per}) *vs.* the one parallel to the beam axis for the heavier fragment of the two from the PLF break-up, for different selections of PLF break-up asymmetry A_H/A_L. Right (4 panels): same as left panels but for the lighter fragment.

$100 \leq A_H + A_L \leq 134$, where H stays for Heavy and L for Light, and the parallel velocity of their source, their c.m. ref. sys, to be greater than 5 cm/ns. To avoid contaminations from fusion-fission reactions, we reconstructed the PLF kinetic energy prior to the break-up and, from this, the one of the undetected in most of the cases TLF, and required the reconstructed TKE to be greater than 1650 MeV, well above the TKE of fusion-fission reactions as seen in fig. 2. By using, as a test sample, the ternary events where the two fragments of PLF break-up and the TLF were detected, we have tested that the reconstructed TKE is in good agreement with the one properly measured in those complete events. As a further check, we have verified that in the selected events, the region of the reconstructed PLF is, in the A *vs.* v_{par} space, quite separated from one of the fusion-fission events shown in the right panels of fig. 2.

By selecting in this way the PLF break-up events following DIC, we have analysed them to some preliminary extent. The four left panels of fig. 3 show the component of velocity perpendicular to the beam direction, v_{per}, *vs.* the v_{par} of the heavier fragment coming from the PLF break-up, as depending on the PLF break-up asymmetry A_H/A_L, while the four right panels present the same but for the lighter one. In all the cases we see the characteristic pattern of the Coulomb-ring, the lighter the fragment the wider the Coulomb-ring, as expected by the interplay of Coulomb repulsion and momentum conservation in the two-body process. Some irregularities due to the partial coverage of the phase space, due to not operative detectors and to the lack of FARCOS data (not included here), can be noticed. We can see that for more symmetric break-up, the population of the rings tends to be forward-backwards symmetric, as expected for equilibrated/slow break-up, while for more asymmetric splitting we see signs of forward-backwards asymmetry, as expected for fast-dynamical break-up, as already seen in the study of PLF break-up at 35 A MeV. To be more quantitative, we have then extracted the $\cos(\theta_{prox})$ angular distributions, as proposed in [20] and extensively used in our previous works, presented in the left panel of fig. 4. While for more symmetric splitting

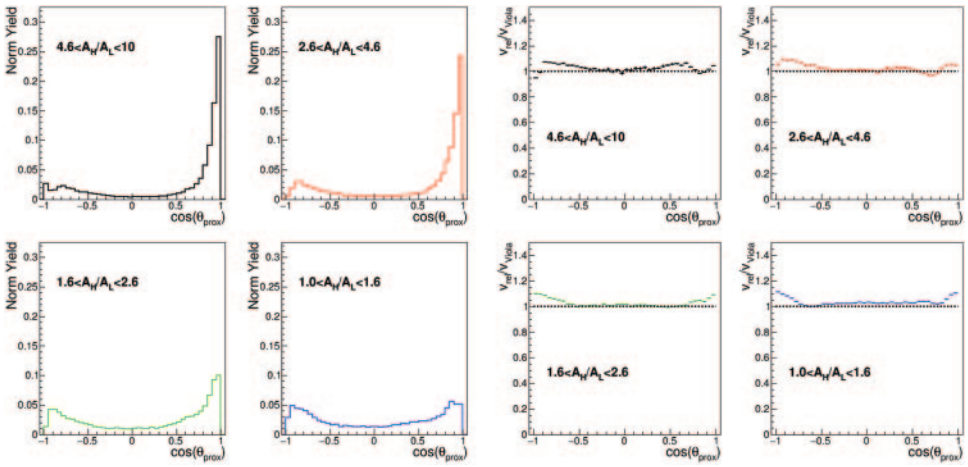

Fig. 4. – (Color online) Left (4 panels): $\cos(\theta_{prox})$ distribution for different selections of PLF break-up asymmetry. Right (4 panels): mean value of the relative velocity, normalized to the one given by Viola systematics, as a function of $\cos(\theta_{prox})$ values, for different selections of PLF break-up asymmetry.

a forward-backwards symmetric, around zero, distribution is obtained, increasing the splitting asymmetry we see an increase of the forward-backward asymmetric contribution coming from the fast-dynamical PLF break-up. The percentage ascribable to the dynamical emission has then been extracted using the method described in ref. [9] and it is reported in table I; the behaviour is similar to the one already observed at 35 AMeV but the strength of dynamical effects seems to be lower here at 20 AMeV, even if this has to be confirmed after correcting the data for experimental efficiency. In the table also results obtained with the same beam, but with neutron poorer target of ^{64}Zn, as obtained by using the same analysis scheme, are given. We can notice, despite the small difference, the trend of a lower presence of dynamical effects for the neutron poor target; this is in agreement with the finding of ref. [9] where, at the beam energy of 35 AMeV, was demonstrated that the strength of dynamical effects increases with, both and separately, the N/Z content of projectile and target; it is of some relevance to see the confirmation of our previous result at different beam energy. The analysis of other projectile/target combinations of the CHIFAR experiment will give, in the future, more information on this issue.

TABLE I. – *Percentage of Dynamical emission as a function of PLF mass splitting asymmetry A_H/A_L for the ^{124}Sn+^{64}Ni and ^{124}Sn+^{64}Zn reactions at 20 AMeV.*

	Dynamical emission (%)	
A_H/A_L	^{124}Sn+^{64}Ni	^{124}Sn+^{64}Zn
4.6–10	52	45
2.6–4.6	48	43
1.6–2.6	22	18
1.0–1.6	5	4

Finally, in the right panels of fig. 4 we show the mean value of relative velocity between the two PLF break-up fragments, normalized to Coulomb repulsion as given by the Viola systematics, as a function of the $\cos(\theta_{prox})$ variable. The fact that normalized relative velocity stays around one in the angular region typical of equilibrated emission is in line with expectations and it probes the goodness of velocity calibration through the E-ToF technique. In agreement with what previously observed at 35 AMeV, we see an increase of relative velocity for aligned emission with the heavy fragment forward emitted, *i.e.*, toward $\cos(\theta_{prox})$ equal to one. However, the extra-velocity, with respect to the one due to Coulomb repulsion, is quite small ($\sim$10%) compared to what observed at 35 AMeV; this indicates that the neck-emission mechanism, the one where higher deviation from Viola systematics is expected due to the almost equal degree of correlation of the IMF with both the PLF and the TLF, is less relevant here and a description based on fission-like break-up appears to be more appropriate. Moreover, deviations from Viola systematics are here observed also toward $\cos(\theta_{prox})$ equal to minus one, the case where is the lighter of the two fission-like fragments to be forward emitted. Also, this gives indications towards a prevalence of dynamical effects due to shape-instabilities, where the strong deformations or shape oscillations drive the PLF fast break-up, rather than the bulk effects of the neck emission mechanism. However, these findings need to be confirmed by more stringent and detailed results.

Concluding, the preliminary analysis of this new data at 20 AMeV incident energy has shown promising results, showing competition of mechanisms, as expected, and the persistence and confirmation of effects and findings already observed at the previously studied energy of 35 AMeV. However, also some relevant differences, related to the lower energy regime here explored, seem to emerge. More complete and refined results, extended also to other projectile/target combinations, will be available in the future and will allow to better study the investigated topics.

REFERENCES

[1] De Filippo E. and Pagano A., *Eur. Phys. J. A*, **50** (2014) 32.
[2] De Filippo E. *et al.*, *Phys. Rev. C*, **71** (2005) 044602.
[3] Papa M. *et al.*, *Phys. Rev. C*, **75** (2007) 054616.
[4] Pagano A. *et al.*, *Eur. Phys. J. A*, **56** (2020) 102.
[5] De Filippo E. *et al.*, *Phys. Rev. C*, **86** (2012) 014610.
[6] De Filippo E. *et al.*, *Phys. Rev. C*, **71** (2005) 064604.
[7] Russotto P. *et al.*, *Phys. Rev. C*, **81** (2010) 064605.
[8] Russotto P. *et al.*, *Phys. Rev. C*, **91** (2015) 014610.
[9] Russotto P. *et al.*, *Eur. Phys. J. A*, **56** (2020) 12.
[10] Geraci E. *et al.*, *Nucl. Phys. A*, **732** (2004) 173.
[11] Pagano A. *et al.*, *Nucl. Phys. A*, **681** (2001) 331.
[12] Pagano A., *Nucl. Phys. News*, **22** (2012) 28.
[13] Pagano E. V. *et al.*, *EPJ Web of Conferences*, **117** (2016) 10008.
[14] De Filippo E. *et al.*, *Eur. Phys. J. A*, in preparation.
[15] Casini G. *et al.*, *Phys. Rev. Lett.*, **71** (1993) 2567.
[16] Stefanini A. A. *et al.*, *Z. Phys. A*, **351** (1995) 351.
[17] Pagano E. V. *et al.*, these proceedings.
[18] Gnoffo B. *et al.*, LNS Activity Report 2020 (2021) p. 91; Russotto P. *et al.*, *Nucl. Instrum. Methods A*, in preparation.
[19] Viola V. E. *et al.*, *Phys. Rev. C*, **31** (1985) 1550; Hinde D. J. *et al.*, *Nucl. Phys. A*, **472** (1987) 318.
[20] Bocage F. *et al.*, *Nucl. Phys. A*, **676** (2000) 391.